General Disclaimer

One or more of the Following Statements may affect this Document

- This document has been reproduced from the best copy furnished by the organizational source. It is being released in the interest of making available as much information as possible.

- This document may contain data, which exceeds the sheet parameters. It was furnished in this condition by the organizational source and is the best copy available.

- This document may contain tone-on-tone or color graphs, charts and/or pictures, which have been reproduced in black and white.

- This document is paginated as submitted by the original source.

- Portions of this document are not fully legible due to the historical nature of some of the material. However, it is the best reproduction available from the original submission.

Contract No: NAS 9-16473
DRL No: T-1691
Line Item No: 1
DRD No: MA 129T

CR-171 734

Investigation of Digital Encoding Techniques for Television Transmission

Final Report

NASA Johnson Space Center
Houston, Texas 77058

December 15, 1983

Donald L. Schilling
Professor of Electrical Eng.
Principal Investigator

COMMUNICATIONS SYSTEMS LABORATORY
DEPARTMENT OF ELECTRICAL ENGINEERING
The City College of
The City University of New York

THE CITY COLLEGE OF
THE CITY UNIVERSITY of NEW YORK

Contract No: NAS 9-16473
DRL No: T-1691
Line Item No: 1
DRD No: MA 129T

Investigation of Digital Encoding Techniques for Television Transmission

Final Report
December 15, 1983
NASA Johnson Space Center
Houston, Texas 77058

Donald L. Schilling
Principal Investigator
Department of Electrical Eng.

COMMUNICATIONS SYSTEMS LABORATORY
DEPARTMENT OF ELECTRICAL ENGINEERING
The City College of
The City University of New York

ABSTRACT

NTSC composite color television signals are sampled at four times the color subcarrier and transformed using intraframe two dimensional Walsh functions. We show that by properly sampling a composite color signal and employing a Walsh transform the YIQ time signals which sum to produce the composite color signal can be represented, in the transform domain, by three component signals in space. By suitably zonal quantizing the transform coefficients the YIQ signals can be processed independently to achieve data compression and obtain the same results as component coding. Computer simulations of three bandwidth compressors operating at 1.09, 1.53 and 1.8 bits/sample are presented. The above results can also be applied to the PAL color system.

TABLE OF CONTENTS

I. Introduction

The image processing facility at the Communications Laboratory of the City College of New York was used to investigate low bit rate, intraframe, video bandwidth compression techniques. Both Hadamard transform and predictive coding techniques were computer simulated and subjectively compared. A predictive coder with a delta modulator quantizer was implemented in hardware.

II. Video Bandwidth Compression Algorithms

Three algorithms were computer simulated and compared. The characteristics of the algorithms are sumarized below. A detailed description of the algorithms are given in appendix A and B.

A. Hadamard Transform Coding

1. The transform operated on the composite NTSC signal sampled at 4 times the color subcarrier frequency (14.3 MHz).

2. The transform was two dimentional, intra field, and non-adaptive.

3. The bandwidth compressed bit rate was chosen to be 21.5 MB/sec.

B. Delta Modulator

1. The input signal was a composite NTSC color signal.

2. The sampling rate and the transmitted bit rate

was set at 21.5 MB/sec (6 times the color subcarrier frequency).

3. The predictor used eight past samples from the current scanning line and was adaptive.

C. Adaptive DPCM

1. The imput signal was a composite NTSC color signal sampled at 10.7 MHz (3 times the color subcarrier frequency).

2. The predictor used 4 past samples from the current scanning line and was adaptive.

3. The quantizer was adaptive and generated 2 bits (4 quantization levels) per sample.

4. The transmission bit rate was 21.5 MB/sec.

III. Real Time Video Bandwidth Compressor

A real time adaptive delta modulator (ADM) was built and subjectively evaluated. The specifications of the ADM were given in section II B. A detailed description of the algorithm, block diagrams and circuit schematic of the coder are given in appendix A.

IV. Results

A comparison of the three coding algorithms have revealed the following

1. At low bit rates, less than 21 MB/s, transform coding produced the best subjective pictures.

2. At 21 MB/s the delta modulator (ADM) produced

the same quality pictures as an adaptive DPCM coder. (See appendix A).

3. At 21 MB/s the ADM picture quality was sufficient for many teleconferencing applications.

IV.

Appendix A

ABSTRACT

Predictors operating on video signals sampled at 6 times the color subcarrier ($6f_c$) have been investigated and compared with predictors operating at 3 times the color subcarrier ($3f_c$). When the best $6f_c$ predictor is used with an adaptive delta modulator (ADM) step size generator, the resulting pictures are similar in quality to $3f_c$ predictors operating with a four level adaptive DPCM quantizer.

An ADM coder was implemented in real time. The coder used between 24 and 34 IC's, depending upon the algorithm, and fits on a single 9"x6" PC board. The transmission rate is 21.4 Mb/s. Subjective evaluation of the coder revealed that the picture quality was sufficient for many teleconferencing applications.

COMPOSITE NTSC COLOR VIDEO BANDWIDTH COMPRESSOR

I. Introduction

The research presented in this paper was motivated by the need to design a simple, low cost, digital, video bandwidth compressor that would produce teleconferencing quality pictures. The bit rate was set at 21.4MB/s to allow two TV signals to be sent over a single T3 telephone line or 36 MHz satellite link.

Most of the recent literature on video bandwidth compression has been concerned with the design of very complex encoders whose implementation requires a rack of equipment. In this paper we present a video bandwidth compressor that was constructed from the standard 100K series ECL IC's and fits on a 9 x 6 PC board.

The need to keep the coder simple and low cost precluded the use of any compression technique other than intraframe predictive coding. A choice between composite or component coding, and a choice between one or two dimentional prediction remains. Since most video sources are in composite form, the extra circuitry needed to generate the components from a composite source mediated in favor of a composite coder. A two dimentional predictor requires at least one scanning line of memory and it also requires that the sampling clock of the coder be synchonized to the horizontal sync or to the burst. Neither is needed for one dimensional prediction. Complexity was the deciding factor, and one dimentional prediction was chosen.

Two schemes were considered for implementation in hardware. One was a DPCM coder that used an adaptive quantizer (ADPCM). The ADPCM coder would sample the video signal at 10.7 MHz ($3f_c$) and transmit 2 bits per sample. The other scheme was an adaptive delta modulator (ADM). The ADM would sample the signal at 21.4 MHz ($6\ f_c$) and transmit 1 bit per sample. Both schemes would transmit at the same rate, 21.4 MB/s.

The ADM uses a predictor for which the composite video signal is sampled at $6\ f_c$. To the best of the authors' knowledge no prior work has been done on predictors at a sampling rate of 6 fc.

Fig. 1a is a block diagram of the adaptive delta modulator (ADM) and Fig. 1b is a block diagram of the adaptive DPCM coder (ADPCM). The symbols used in Fig. 1 are used throughout the rest of the paper.

II. ADM Predictor (6 x color subcarrier)

This section presents the derivation of the predictors which use a composite video signal sampled at 6 times the color subcarrier ($6f_c$). Fig. 2 shows the location of the samples in the picture with respect to the color subcarrier. Fig. 2 was drawn for constant luminance and chrominance. X is the pel to be predicted. P is the predictor's estimate of X. P is formed from a weighted sum of past pels as shown in Eq. 1 and Fig. 1

$$P = aA + bB + cC + eE + fF + gG + hH + \ldots \qquad (1)$$

where:

A,B,C...are the inputs to the predictor

a,b,c...are the prediction coefficients for pels A,B,C..

A predictor that sets P equal to sample X, (see Fig. 2) is a reasonable predictor. The values of the prediction coefficents that set P = X in Eq. 1 for the conditions of Fig. 2 can be found as follows: Let the luminance of all the pels equal α, let the phase angle of the subcarrier be θ with respect to the sampling clock, and let the amplitude of the subcarrier be β, then the pels X and A through H are given by:

$X = \alpha + \beta\cos\theta$

$A = \alpha + \beta\cos(\theta + 300) = \alpha + .5\,\beta\cos\theta + .5\sqrt{3}\,\beta\sin\theta$

$B = \alpha - .5\,\beta\cos\theta + .5\sqrt{3}\,\beta\sin\theta$

$C = \alpha - \beta\cos\theta$

$D = \alpha - .5\,\beta\cos\theta - .5\sqrt{3}\,\beta\sin\theta$

$E = \alpha + .5\,\beta\cos\theta - .5\sqrt{3}\,\beta\sin\theta$

$F = \alpha + \beta\cos\theta$

$G = A$

$H = B$

Substituting the values of the pels A through H into Eq. 1 and setting P = X yields:

$$P = X = \alpha + \beta\cos\theta = a(\alpha + .5\beta\cos\theta + .5\sqrt{3}\beta\sin\theta) +$$
$$b(\alpha - .5\beta\cos\theta + .5\sqrt{3}\beta\sin\theta) + c(\alpha - \beta\cos\theta) +$$
$$d(\alpha - .5\beta\cos\theta - .5\sqrt{3}\beta\sin\theta) +$$
$$e(\alpha + .5\beta\cos\theta - .5\sqrt{3}\beta\sin\theta) +$$
$$f(\alpha + \beta\cos\theta) + g(\alpha + .5\beta\cos\theta + .5\sqrt{3}\beta\sin\theta) +$$
$$h(\alpha - .5\beta\cos\theta + .5\sqrt{3}\beta\sin\theta) \qquad (2)$$

If the left side of Eq. 2 is to equal the right side for all values of α, β and θ three conditions must be met: 1) The sum of all terms containing α on the right side of Eq. 2 must sum to α; 2) The sum of all terms containing $\sin\theta$ must sum to zero; and 3) The sum of all terms containing $\beta\cos\theta$ must sum to $\beta\cos\theta$. These three conditions give rise to equations 3, 4 and 5:

$$a + b + c + d + e + f + g + h = 1 \qquad (3)$$
$$a + b + \emptyset - d - e + \emptyset + g + h = \emptyset \qquad (4)$$
$$a - b - 2c - d + e + 2f + g - h = 2 \qquad (5)$$

Since there are only three equations and many unknowns there are an infinite number of solutions to Eqs. 3 - 5. Several solutions are listed below with the values for a, b, c... substituted back into Eq. 1.

I. $P = 2A - 2B + C$

II. $P = 1.5A - B + .5D$

III. $P = A + D - C$

IV. $P = A - .25B + .5E - .25H$

V. $P = A - .25B - .5C + .5D + .25E$

VI. $P = .65A + .05B - .4C + .05D + .65E$

VII. $P = F$

The predictors listed above are referred to as subcarrier predictors because they were derived so as to predict the values of the samples along a constant subcarrier.

The following comments can be made regarding the predictors. Predictor I uses the most recent pels, and therefore, it should be able to respond well to sudden changes in the picture. For predictor VI the sum of the squared values of the prediction coefficients are equal to 1, which is less than all other predictors except predictor VII. Small prediction coefficients are important since the quantization noise in the encoded pels A, B, C.... is multiplied by their respective coefficients. If the quantization noise of each encoded pel is independent and of equal variance, then the quantization noise in P will be proportional to the sum of the squared values of the prediction coefficients.

Subcarrier predictors produce prediction errors during and shortly after step changes in luminance. To minimize this problem we introduced the edge predictor, predictor VIII, shown below:

VIII $P = A$

The hypothesis behind predictor VIII is that the previously estimated sample is a better predictor than a subcarrier predictor when there is a sudden change in luminance.

The edge predictor can be combined with any subcarrier predictor by introducing the parameter N. Eq. 6 thru 8 show the resulting predictor. When N=1 Eq. 8 reduces to the subcarrier predictor and when N=Ø Eq. 8 reduces to the edge predictor.

$$P = (1-N)(\text{EDGE PREDICTOR}) + N(\text{SUBCARRIER PREDICTOR});\ \emptyset < N < 1 \quad (6)$$

$$P = (1-N)A + N(aA + bB + cC + \ldots);\ \emptyset < N < 1 \quad (7)$$

$$P = (1+N(a-1))A + N(b\,B + c\,C + \ldots);\ \emptyset < N < 1 \quad (8)$$

Eq. 6 - 8 are equivalent. The value assigned to N is discussed in sections IV and VII.

III. ADPCM Predictor (3 x color subcarrier)

A similar analysis to the one presented for the $6f_c$ (ADM) predictor can be carried out for the ADPCM predictor. Since the ADPCM coder samples at $3f_c$, only samples B, D, F and H are available. (See Fig. 2). Eqs. 3 - 5 yield only one solution and it has the form:

$$P = F + (B-H)\Delta \qquad ;\ \Delta \text{ can be any number}$$

The value of Δ that minimized the mean square prediction error for the test pictures in Fig. 3 is Ø.8. This results in predictor IX.

IX $\quad P = .8B + F - .8H$

The terms in predictor IX have the following interpretation. Sample F is a perfect predictor for X when

the luminance and chrominance remain constant. When the luminance changes, the term (B-H)(.8) adds a slope correction factor to F.

IV. Predictor Performance Results

The predictors were evaluated using the test pictures shown in Fig. 3. The evaluation was carried out without a quantizer. The performance criteria is a normalized predictor gain [2] which is defined as the ratio of the peak-to-peak signal power to the mean square error signal. Mathematically the performance criteria has the form of a signal-to-noise ratio and is given by:

$$\text{PRED. GAIN} = 10 \text{ LOG} \left[\frac{S_{pp}^2}{\frac{1}{M} \sum_{i=1}^{M} (X_i - P_i)^2} \right] \qquad (9)$$

S_{pp} = the peak-to-peak signal amplitude and is equal to 256.

X_i = the i^{th} picture sample

P_i = the prediction of sample X_i (See equation 1)

M = the number of samples in the picture

The larger the PRED GAIN the better the predictor.

The results from testing the predictors without a quantizer are shown in TABLE I. TABLE I shows the PRED GAIN when the optimum value of N is used in Eq. 8 with predictors I thru VI. An attempt was made to increase the prediction gain over that obtained from the optimum value of N by

TABLE I - Predictor Evaluation Without a Quantizer

PREDICTOR	OPTIMUM N*	PRED. GAIN**
I	N=.9	35.8
II	N=.9	34.8
III	N=.9	33.0
IV	N=.85	33.5
V	N=.85	32.5
VI	N=.75	30.9
VII	Not Applicable	24.4
VIII	Not Applicable	27.8
IX	Not Applicable	28.3
P=B	Not Applicable	23.0

* The relationship between N and the predictor is shown in equations 6,7 and 8

** PRED. GAIN is defined in equation 9

making N variable. N was set to be a monotonically decreasing function of $|A - G|$. The hypothesis is that the value of $|A - G|$ is an indication of an edge. When $|A - G|$ is large N should be small so that Eq. 6 gives more weight to the edge predictor, and when $|A - G|$ is small more weight is given to the subcarrier predictor. With a variable N the prediction gain increased by only .1db to 1db (depending upon the predictor) over the best fixed N.

The ADM predictors that relied on the most recent pels did the best. Unfortunately these predictors also had the largest prediction coefficients and as a result they did not do the best when a quantizer was added.

V. ADPCM Quantizer

The quantizer for the ADPCM coder is adaptive [3]. The way in which the quantization levels adapt is shown in Fig. 4. At each sampling instant, k, the quantizer has one of four values to choose from, such that

$$-q_2(k) < -q_1(k) < q_1(k) < q_2(k)$$

The quantizer will choose the value of q(k) that minimizes $|\hat{x}_{k+1} - x_{k+1}|$. If the quantizer chooses either of the outer values, $\pm q_2(k)$, at time k then at time k+1 the quantizer will have a larger set of values to choose from such that $q_2(k+1) > q_2(k)$ and $q_1(k+1) > q_1(k)$. If the quantizer chooses either inner value, $\pm q_1(k)$, at time k, then at time k+1 the quantizer will have a smaller set of values to choose from such that $q_2(k+1) < q_2(k)$ and $q_1(k+1) < q_1(k)$. The

quantizer values are given by the following expressions:

$$|q_2(k)| = \varepsilon |q_1(k)|$$

$$\left.\begin{aligned} |q_2(k+1)| &= P|q_2(k)| \\ |q_1(k+1)| &= P|q_1(k)| \end{aligned}\right\} \text{If the quantizer chose } \pm q_2(k) \text{ at time k.}$$

$$\left.\begin{aligned} |q_2(k+1)| &= Q|q_2(k)| \\ |q_1(k+1)| &= Q|q_1(k)| \end{aligned}\right\} \text{If the quantizer chose } \pm q_1(k) \text{ at time k.}$$

$\varepsilon = 3.5$

$P = 2.6$

$Q = 0.9$

$q_1(\min) = 2$

$q_2(\max) = 31$

ε, P and Q were optimized for the pictures shown in Fig. 4 for a sampling rate of 10.7 MHz ($3f_c$).

The quantizer transmits 2 bits to the receiver for each picture sample. The first bit, e_1, carries the sign of q(k) and second bit, e_2, signals the generation of $q_1(k)$ or $q_2(k)$.

VI. ADM Quantizer

The quantizer for the ADM coder is the ADM step size generator described by Song [4]. It is sometimes referred to as a P, Q delta modulator because the step size increases by the factor P or decreases by the factor Q. The ADM coder

can be described by Eq. 10 - 14.

$$P_K = \sum_{i=0}^{l} a_i X_{k-i} \quad ; \; a_i \text{ is the } i^{th} \text{ prediction coefficient} \tag{10}$$

$$E_{k+1} = \text{Sign}\{X_{k+1} - (P_k + \emptyset.1\, E_k |Y_{k-1}|)\} \tag{11}$$

$$Y_k = |Y_{k-1}|(1.13E_k + .29\, E_{k-1}) \tag{12}$$

$$\left.\begin{aligned} Y_{k(\min)} &= 2 \\ Y_{k(\max)} &= 31 \end{aligned}\right\} \tag{13}$$

$$\hat{X}_{k+1} = P_k + Y_k \tag{14}$$

where the above variables are defined in Fig. 1b.

When $E_k = E_{k-1}$ in Eq. 12, the step size Y_k, increases by the factor P = 1.4 and when $E_k = E_{k-1}$, Y_k decreases by the factor Q = .84. The constants in Eqs. 10-14 were optimized for the pictures shown in Fig. 3 for a sampling rate of 21.4 MHz ($6f_c$).

VII. Results of ADM and ADPCM Coding

This section gives the results of the evaluation of the predictors with quantizers. The performance criteria is a signal to noise ratio which is defined as the ratio of the peak to peak signal power to the filtered mean square error signal. The error signal (defined as $\hat{}_{k+1}$ $_{k+1}$) is filtered to eliminate the energy from out of band frequency components. These components stretch from 4.2 MHz to one half the sampling rate. The filters used to eliminate the out of band frequency components from the error signal were 5 pole butterworth filters with a cutoff frequency of 4.2

MHz. If the filtered error signal is denoted as EF, then the performance criteria is given by:

$$S/N = 10 \text{ LOG } \frac{S_{pp}^2}{\frac{1}{M}\sum_{i=0}^{M}(EF)^2} \qquad (15)$$

where $(EF)_i$ is the i^{th} filtered error signal. M and S_{pp} are defined for Eq.9.

The results of ADM and ADPCM coding for the various predictors are given in Table II. A comparison of the predictors for $6f_c$ sampling with and without the ADM quantizer reveals that the ADM quantizer has a significant effect on relative predictor performance. Table I shows predictor I to be the best predictor, but Table II reveals it to be among the worst predictors when a quantizer is added. This is probably due to its large prediction coefficients. Predictor VI is among the worst predictors in Table I (probably because of the small prediction coefficients of pel A) but it is among the best in Table II (probably because the sum of the squared values of the prediction coefficients are very small). The best predictor with an ADM quantizer is predictor IV. The reason for this is uncertain but it is probably due to the following factors: The coefficents are small; the most recent pel, A, is weighted more than any other pel, and it behaves well on slopes. If pels A thru H lie on a straight line of arbitrary slope then P will equal pel A for predictor IV.

A subjective comparison between the ADM quantizer

TABLE II - Predictor Evaluation With A Quantizer

PREDICTOR	QUANTIZER	N	S/N from Eq. 15
I	ADM	N=1 N*=.63	17.5 32.1
II	ADM	N=1 N*=.56	28.1 32.8
III	ADM	N=1 N*=.41	28.4 32.0
IV	ADM	N=1 N*=.73	34.2 34.4
V	ADM	N=1 N*=.62	30.5 33.1
VI	ADM	N=1 N*=.58	29.6 33.2
VII	ADM	N.A.	26.6
VIII	ADM	N.A.	30.8
VII	ADPCM	N.A.	30.7
IX	ADPCM	N.A.	34.7
P=B	ADPCM	N.A.	31.9

* Optimum value for N

with predictor IV and the ADPCM quantizer with predictor IX was carried out using the picture processing facilities at The City College of New York. This facility enabled us to computer simulate the ADM and the ADPCM coders for the still pictures in Fig.3 and then display the results on a SONY TRINITRON RECEIVER/MONITOR. Both coders produced the same quality pictures and both exhibited the same type of degradation. The degradation exhibited by the coders was edge busyness. There was no loss of resolution and little graininess except in very highly saturated colors. Contour noise was never visable, even for $Y_{min} = 6$. Apparently the subcarrier acts as an effective dither signal which breaks up any contour noise.

VIII Real Time ADM Coder

A real time ADM coder was built and subjectively evaluated. The ADM coder was chosen over the ADPCM coder because it required fewer IC's to implement. If predictor IV was implemented with N=1 the ADM coder could be constructed with 22 IC's from the ECL 10ØK series, plus a D/A converter and a comparator. An A/D converter is not required. If N was set equal to .75 the IC count would increases from 24 (D/A and comparator included) to 26. If the coder was made programmable so that any value of N could be chosen between Ø and 1 in increments if 1/8 the IC count would increase to 29, and if N was made equal to a function of |A-G| the IC count would increase to 34. The latter coder was built and subjectively evaluated. A block diagram of the coder is shown in Fig.5. The functional relationship

between N and |A-G| is stored in ROM II; therefore, by plugging in different ROMs we could change N. The P and Q values of the step size generator (Eq. 12) were programmed into ROM I. By moving jumper wires we could implement predictors III, IV or V. This large degree of programmability enabled us to check the validity of the computer simulations against a real time coder operating on motion pictures.

The real time subjective evaluations produced no suprises. They tended to confirm the results shown in TABLE II. The entries with the highest signal-to-noise ratios produced the best pictures. When P = 1.4 and Q = .8, N = 3/4 produced slightly better pictures than N =1 for predictor IV. In general, when N was set equal to 1 the picture quality was very sensitive to changes in P, Q and the predictor. When P was increased from 1.4 to 1.5 and Q was reduced from .8 to .5, the picture quality decreased considerably. This was not the case for N = 3/4. Making N a function of |A-G| did not noticeably improve the picture when compared with N = 3/4.

IX Real Time Subjective Evaluation of the ADM Coder

The ADM coder was programmed with PRED IV, N=.75, P=1.4, Q=.8 and subjectively evaluated. The evaluation was performed by a group of viewers seated at a distance of 6 feet from a 19" monitor. The viewers watched several minutes of a daytime soap opera encoded with the ADM. The viewers evaluated the picture by choosing one of the following responses:

1) The picture appears normal, just like a TV picture should appear.
2) The picture appears degraded from a normal TV but the degradation is not annoying.
3) Same as (2) but the degradation is annoying.

Untrained viewers usually chose 1 or 2. The authors chose 2. After seeing the original and encoded pictures side by side most viewers chose option 2. A few chose option 3.

X Conclusions

It is possible to build a digital color TV bandwidth compressor, with a transmission rate of 21.4 Mb/s, out of 26 standard IC's and produce usable quality prictures. The simplicity of the design was acheived by using an ADM step size generator and a novel predictor designed to operate with a sampling rate of 6 times the color subcarrier.

The ADM coder was compared with a DPCM coder which also transmitted at 21.4Mb/s. Both coders produced similar quality pictures but the ADM coder required fewer IC's to implement.

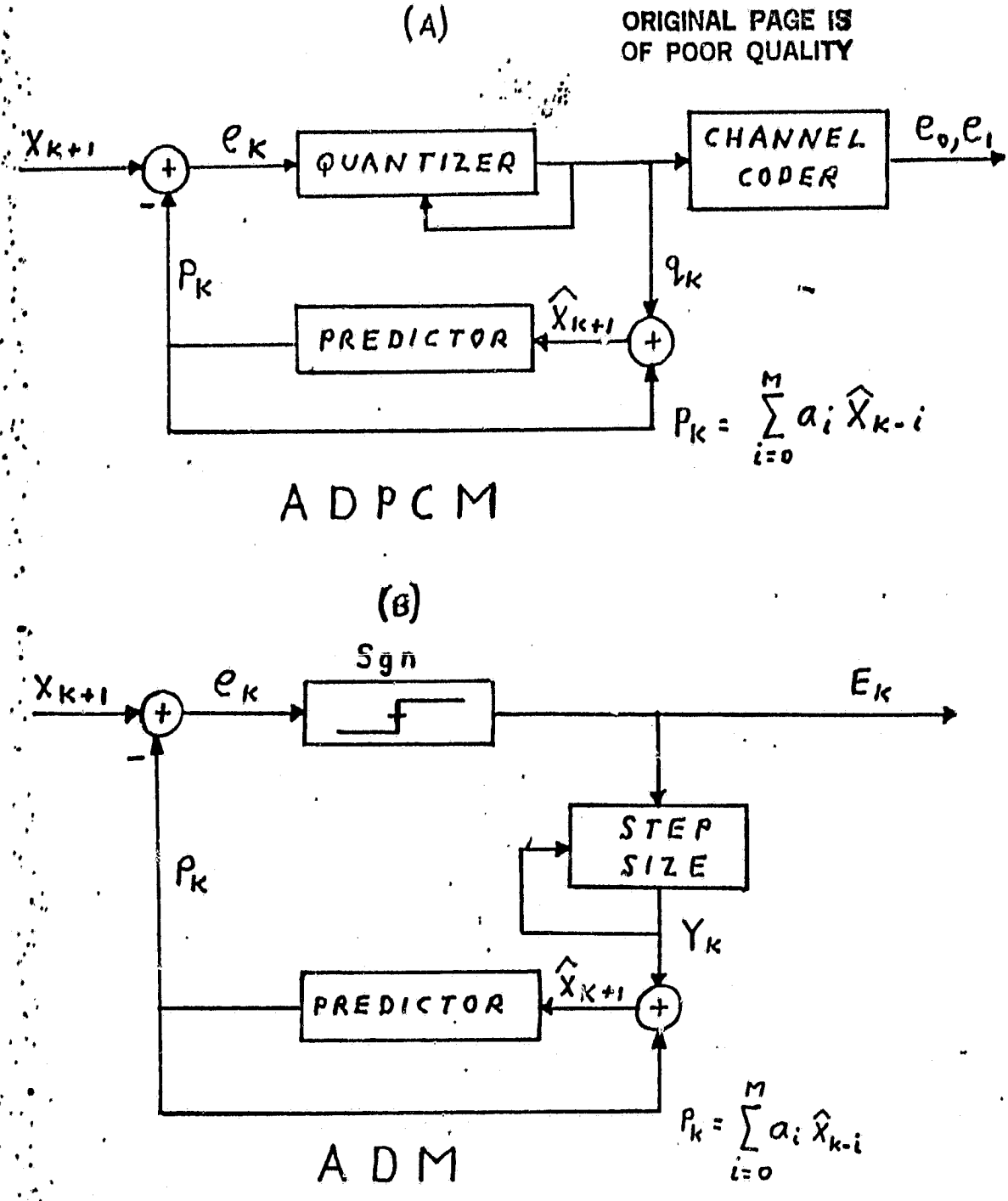

Fig. 1 Block diagram of the ADM coder (a) ; Block diagram of the ADPCM coder (b)

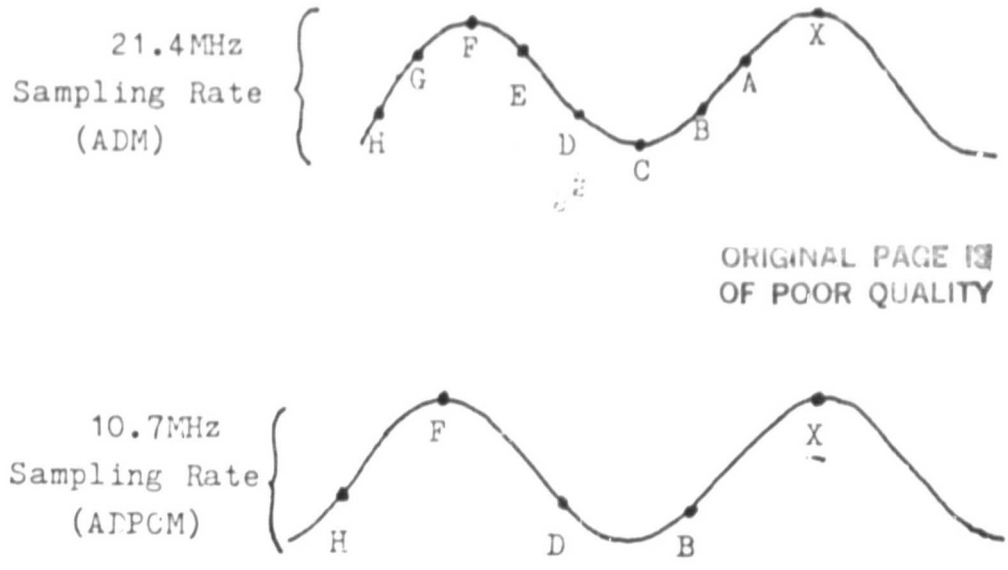

Fig. 2 The figure above shows the location of the pels with respect to the subcarrier.

Fig. 3 Test pictures used for evaluation

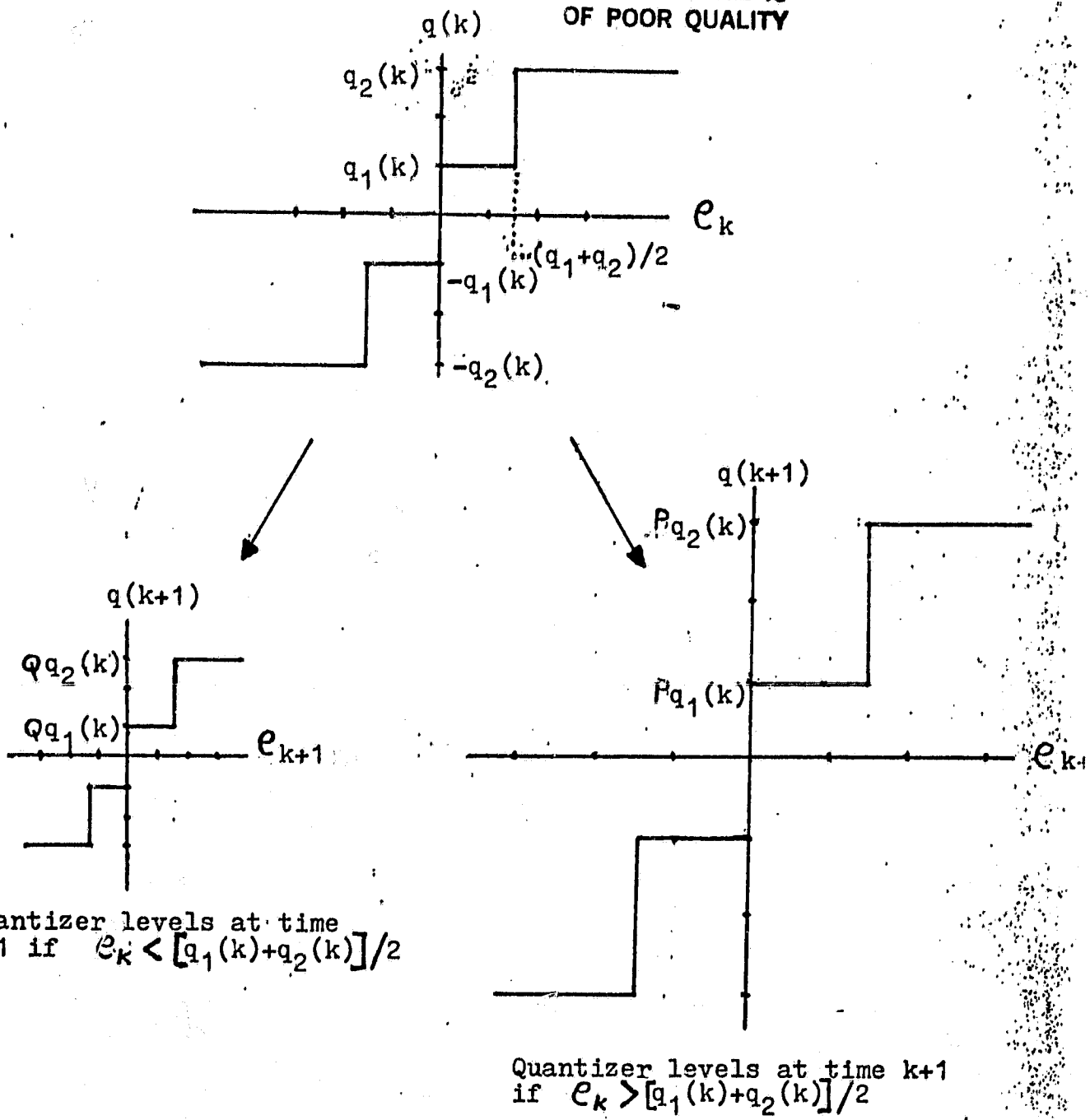

Quantizer levels at time k+1 if $e_k < [q_1(k)+q_2(k)]/2$

Quantizer levels at time k+1 if $e_k > [q_1(k)+q_2(k)]/2$

Fig 4 Adaptive quantizer: The quantization levels expand or compress for each picture sample as shown.

Fig. 5 Block Diagram of the ADM Coder

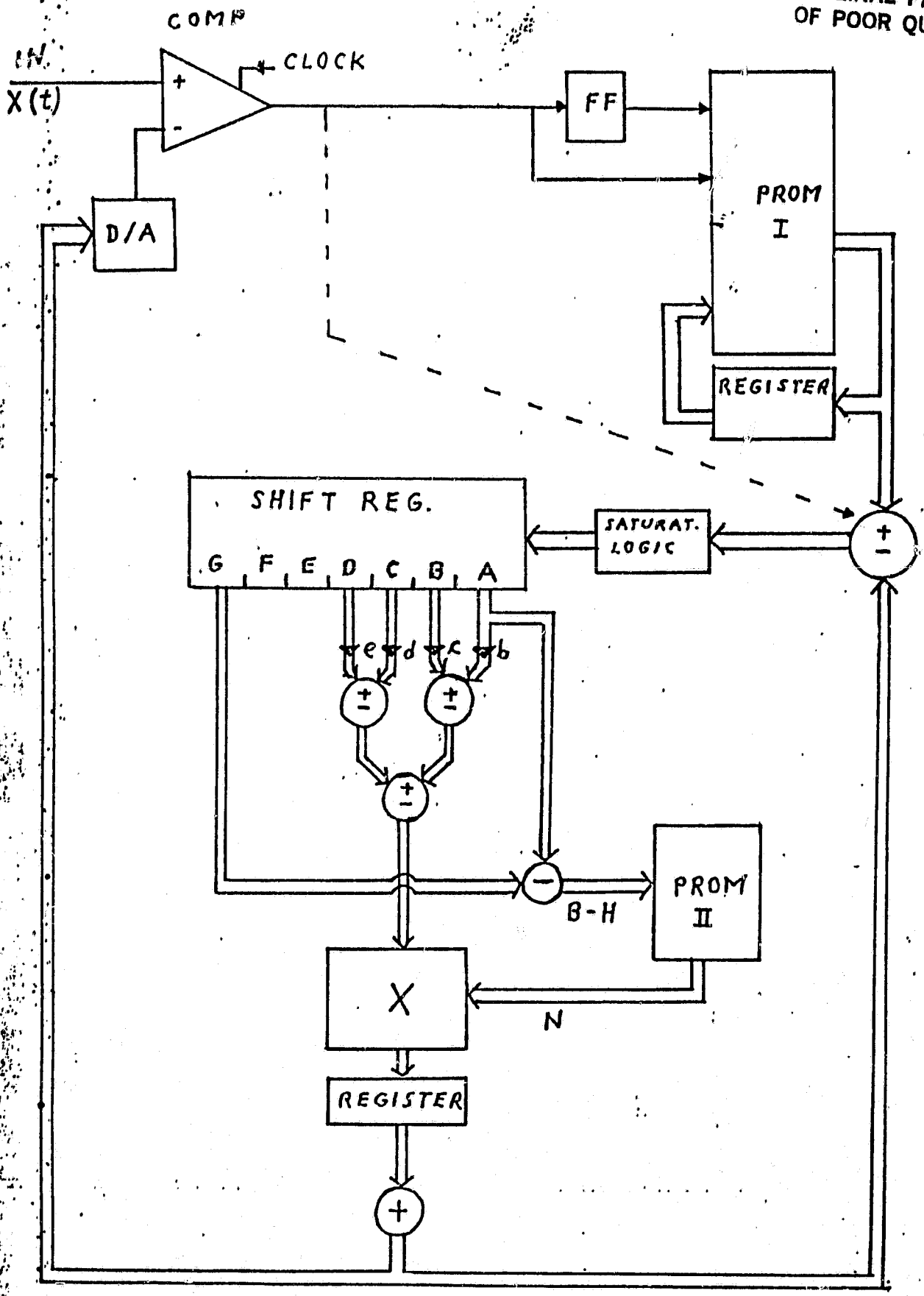

BIBLIOGRAPHY

1. Brainard, Netravali and Pearson, Predictive coding of composit NTSC color television signals, Bell Syst. Tech. J.

2. J. O'Neal, Bounds on subjective performance measures for source encoding systems, IEEE Trans on Info Theory, May 1971

3. N. S. Jayant, Adaptive quantization with a one-word memory, Bell Syst. Tech. J., Sept. 1973

4. Song, Garodnick, Schilling, A variable step size robust delta modulator, IEEE Trans on Comm, Dec. 1971

5. I. Dinstein, DPCM prediction for NTSC composite signals, Comsat Technical Review, Fall 1977

6. V. Devarajan and K.R. Rao, DPCM coders with adaptive prediction for NTSC composit TV signals, IEEE Trans on Comm, July 1980

7. Lei, Scheinberg, Schilling, Adaptive delta modulation systems for video encoding, IEEE Trans on Comm Nov. 1977

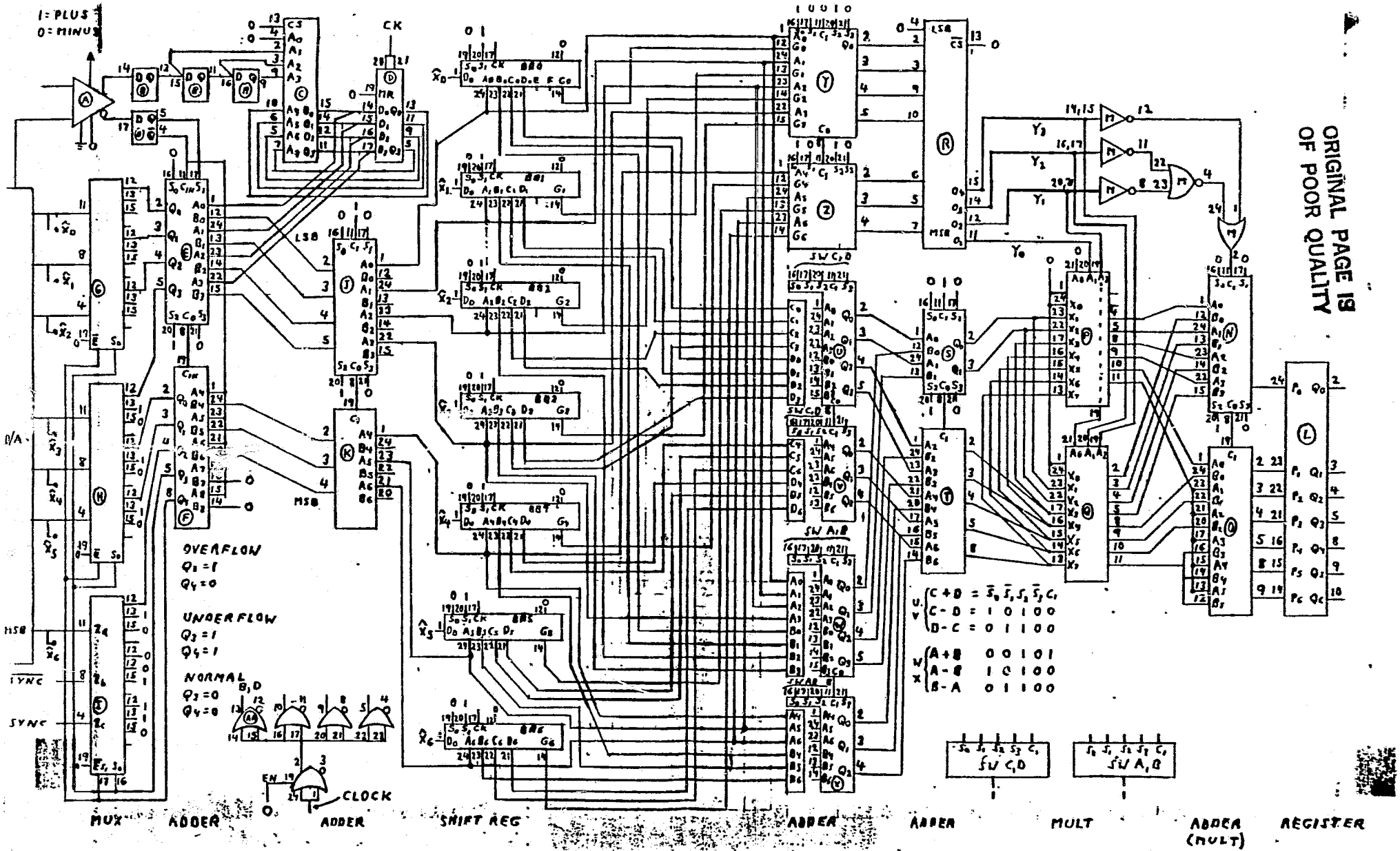

ORIGINAL PAGE IS
OF POOR QUALITY

V.
Appendix B

WALSH TRANSFORM CODING OF NTSC COMPOSITE COLOR SIGNALS

J.B.Bai, J.Barba, N.Scheinberg, D.L.Schilling

City College of New York
Department of Electrical Engineering
New York, New York 10031

ABSTRACT

NTSC composite color television signals are sampled at four times the color subcarrier and transformed using intraframe two dimensional Walsh functions. We show that by properly sampling a composite color signal and employing a Walsh transform the YIQ time signals which sum to produce the composite color signal can be represented, in the transform domain, by three component signals in space. By suitably zonal qunatizing the transform coefficients the YIQ signals can be processed independently to achieve data compression and obtain the same results as component coding. Computer simulations of three bandwith compressors operating at 1.09, 1.53 and 1.8 bits/sample are presented. The above results can also be applied to the PAL color system.

INTRODUCTION

The video images used in this paper were obtained by the system shown in fig.1. The NTSC composite video signals is sampled at four times the color subcarrier and uniformly quantized to 8 bits/sample and stored in the frame freeze unit. The frame freeze can store two frames, each frame consisting of 512 samples/line and 512 lines/frame field interlaced. The computer interface allows images to be transferred between the computer and the frame freeze.

Fig.2 shows the block diagram of the computer simulated system. The frame of video is partitioned into 16x16 sample data matrix upon which the two dimensional Walsh transform operates. In general, let the array f(i,j) represent the samples of an NTSC composite image over an array of N^2 points. Then the two dimensional Walsh transform, F(u,v), of f(i,j) is given by the matrix product

$$[F(u,v)] = \frac{1}{N^2}[H(u,v)][f(i,j)][H(u,v)]$$

where [H(u,v)] is the Hadamard matrix consisting of Walsh functions of order N. The inverse transformation is defined as

$$[f(i,j)] = [H(u,v)][F(u,v)][H(u,v)]$$

The result of the Walsh transform is a 16x16 coefficient matrix where each coefficient represents the projection of the data matrix onto a particular Walsh pattern. Data compression (bandwidth compression) can be achieved because the image energy which is usually uniformly distrubuted in the spatial domain, tends to be concentrated in those transform coefficients which represent the lower frequency component of the Walsh domain. The majority of the other transform coefficients are always nearly zero and need not be transmitted.

The transform coefficients can be partitioned as follows:

1) Luminance information coefficients: These coefficient constitute the majority of the entries in the coefficient matrix and are generally clustered about the low frequency components.

2) The I color signal coefficients: These coefficients always appear in a fix location in the coefficient matrix when the composite signal is properly sampled.

3) The Q color signal coefficients: These coefficients always appear in a fix location in the coefficient matrix when the composite signal is properly sampled.

Typical 16x16 coefficient matrixs are shown in fig.3. The signals described in statements (2) and (3) above can also represent the UV color signals in the PAL system. Which signals are represented in (2) and (3) above will depend on the sampling relative to the color subcarrier.

Thus, the Walsh transform not only maps the time signals into Walsh spectrum signals and compacts the energy distribution, but also acts like a comb filter which seperates the YIQ components of the composite NTSC signals and maps them into specific locations of the coefficient matrix. Note that the Walsh transform can also be used as a color detector since the coefficient which

represents the color information represents the intensity of the baseband color signal.

The process of zonal qunantizing the coefficient matrix consists of first selecting the coefficients to be transmitted and then quantizing the coefficients prior to transmission. The coefficient selection depends on the statistical distribution of the energy in the coefficient matrix. The larger the percentage of the energy contained in the transmitted coefficients, the better the quality of the reconstructed image. The percentage of the energy lost due to those coefficients not selected for transmission is equivalent to the mean square error. Thus, the selection of the coefficients to be transmitted is basically the task of transmitting as much energy as possible in a given bit rate. The quantizer performs both uniform and nonuniform quantization for the coefficients which represent the lower frequency components and those coefficients which represent the higher frequency components respectively. The nonuniform characteristics resemble the Laplace distribution. This results in a trade off between bit rate reduction and reduction in quantization error.

THE WALSH SPECTUM OF I,Q SIGNALS IN THE NTSC COLOR SYSTEM

In the NTSC color system,

$$I = 0.596R' - 0.275G' - 0.321B'$$
$$Q = 0.212R' - 0.523G' + 0.311B'$$

where:

I,Q = the baseband color differential signals
R',G',B' = the tristimulate values gamma corrected signals

A NTSC composite color signal is given by:

$$S = Y + I \cdot \cos(2\pi f_{sc} + 33^\circ) + Q \cdot \sin(2\pi f_{sc} + 33^\circ)$$

where:

S = the NTSC composite color signal
Y = the luminunce signal.
f_{sc} = 3.579545 MHz = (227+1/2)f_h
f_{sc} = color subcarrier.
f_h = the horizontal line frequency.

There are two points that one should note. Firstly, the color signals appear as amplitude modulated waveforms where the amplitudes of the modulated waveform are the baseband color differential signal. Secondly, the phase of the modulated waveforms always change 180° from line to line. When the sampling frequency is equal to four times the color subcarrier and the sampling occurs at 12, 102, 192, and 282 degrees of the subcarrier, the sampled modulated I and Q signals will be as shown in fig.4. Thus, if we consider a 16x16 data matrix in the two dimensional space, the patterns of the modulated signals, I and Q, will be the same as the patterns of the two dimensional Walsh functions (16,9) and (16,8) respectively. In other words, the carrier of the I and Q color information are the same as the two dimensional Walsh functions (16,9) and (16,8). The result is that amplitudes of the modulated I and Q signals will be equal to the values of the coefficients (16,9) and (16,8) in the Walsh domain. If any other data matrix size such as 8x8, 4x4, etc were used, the amplitude of the I and Q signals will also have corresponding coefficients. Just as the modulated I and Q signals have their respective bandwidths in the Fourier domain, the will also have their respective bandwidths in the Walsh domain. The result is that there are coefficients in the Walsh domain which represent the higher components of the I and Q signals as shown in fig.3. The luminance signal, on the other hand, will in gereral not be mapped onto the Walsh patterns (16,8) and (16,9) and thus will not be mapped onto the coefficients in the Walsh domain which correspond to the I and Q signals. This is similiar to what occurs in the Fourier domain where the liminance signal in general does not occupy the same frequency spectrum of the color signals. Thus, the I and Q components of an NTSC composite signal will be mapped onto certain coefficients in the Walsh Coefficients matrix which represents the spectrum of these signals.

If the baseband I and Q signals are seperately sampled at $f_{sc}/4$ and transformed using two dimensional Walsh functions, the energy of the I and Q signals will be compacted into coefficient (1,1) and neighboring coefficients. The coefficients obtained in this manner and those obtained by transforming the NTSC composite signals would be identical. If we transform the baseband signals, for example, the coefficients (1,1), (1,2) and (2,1) which are obtained by transforming the I signal will be equal to coefficients (15,9), (16,10) and (15,9) respectively as shown in fig.3. If an 8x8 Walsh transform is performed on the composite signal the corresponding I components will be (8,5), (8,), (7,5) respectively.

A vector diagram is shown in fig.5. Each color has a prescribed position in the vector diagram. The Q, I

and U, V represent two different coordinate systems. The NTSC system uses the QI coordinates whereas the PAL system uses the UV coordinates. Every color can be represented by its projections along the axis of either of these two coordinate systems or along any other suitable defined set of axis. With reference to fig.5, if the sampling is started at point 1 and continued at 2, 3 and 4 then the coefficients (16,8).... and (16,9).... will be equal to the components of Q and I as stated above. This means that by sampling at this phase relative to the color subcarrier that the basis vectors (16,8) and (16,9) will correspond to the sampled Q and I chrominace signals respectively i.e. the Q signal will be in phase with the vector (16,8) and the I signal will be in phase with the vector (16,9). Note that phase shifts of 90 degress will still produce similar results. In general, the color signal is time varying so that the coefficients (16,8) and (16,9) actually represent the average value of the Q and I signals taken over an area equal to the transform block size. The coefficients (16,7), (15,8),... and (16,10), (15,9),... represent the higher frequency components of the Q and I signals respectively. The sum of the vectors (16,8), (16,7), (15,8),.. is equal to the Q signal just as the sum of the vectors (16,9), (16,10), (15,9),.. is equal to the I signal. The sum of all the vectors in the Walsh domain is equal to the NTSC composite signal.

If the sampling phase relative to the color subcarrier deviates from the above, the basis vectors (16,8) and (16,9) will no longer correspond to the vectors of the the chrominance signals. The result would be that the coefficients (16,8) and (16,9) would now contain components of both the Q and I signals. Thus, if the Q and I signals are not to be seperated then the sampling phase is unimportant. However, the amount of compression is identical in both cases.

To show that the above analysis is correct the NTSC color bars signal was sampled and transformed as described above. The result of this transformation is shown in Table 1. The slight variation of the Q and I signals form the ideal values is due to the sampling phase not being exactly as shown in figs. 4 and 5. However, the results do show that the vectors (16,8) and (16,9) correspond to the Q and I signals.

For the PAL color system the color subcarrier is at a higher frequency than in NTSC and the chrominance signals are not phase shifted by 33 degrees relative to the color subcarrier as in the NTSC system. Consequently, for signals in the PAL system the sampling phase relative to the color subcarrier, required to seperate the chrominance signals in the Walsh domain, should be displaced by 33 degrees relative to the NTSC system, i.e, for the PAL system, sampling should begin at point 1'.

STATISTICAL PROPERTIES OF COEFFICIENTS IN THE WALSH DOMAIN

In order to assign bits to each coefficient in the transform domain and choose quantization characteristics for each coefficient, the energy distribution in the coefficient matrix and the probability density of each coefficient were considered. The energy density distribution in the Walsh domain is defined as:

$$ED(i,j) = \frac{\sum_{m=1}^{B}\sum_{n=1}^{B} V_{mn}^2(i,j)}{\sum_{m=1}^{B}\sum_{n=1}^{B}\sum_{i=1}^{W}\sum_{j=1}^{W} V_{mn}^2(i,j)}$$

where:

ED(i,j) = energy density of coefficient (i,j). This is averaged over the entire image.
V(i,j) = the value of coefficient (i,j).
(i,j) = the elements in the coefficient matrix.
W = the size of the matrix used.
B^2 = the total number of matix in the partioned image.

The average value of each coefficient is given by:

$$AV = \frac{1}{B^2}\sum_{m=1}^{B}\sum_{n=1}^{B} V_{m,n}(i,j)$$

and the coefficient variance is given by:

$$VA(i,j) = \frac{1}{B^2}\sum_{m=1}^{B}\sum_{n=1}^{B} [V_{mn}(i,j)-AV(i,j)]^2$$

The statistical results obtained from various different types of images indicate that the picture energy is compacted into those coefficients which represent the lower frequency components such as coefficients (1,1), (1,2), (2,1) and those coefficients which represent the color information such as

coefficients (16,8) and (16,9), as shown in fig.6. In fig.6, the darker areas in the figure represent the greater energy density. Also, the coefficients which contain the same energy form hyperbolas in the coefficient matrix. The energy density of the SMPTE #1 test slide is shown in fig.7.

The average values of coefficients (1,1), (16,8) and (16,9) represent the average intensity of luminence, Q and I signals respectively. The other coefficients have nearly zero average value. The coefficients (1,1), (16,8) and (16,9) also have the greatest change in variance whereas the other coefficients have much smaller changes in variance.

The energy density distribution is one of the basic factors used to select those coefficients which are to be transmitted. Those coefficients which contain zero or almost zero energy density are not transmitted. In order to obtain the optimal bit assignment, the number of bits assigned to each coefficients is proportional to its variance. In this paper, the number of bits assigned to each coefficient were calculated by the equation:

$$B(i,j) = \log_2[|AV(i,j)| + 3 \cdot VA^{\frac{1}{2}}(i,j)|] + 1$$

The B(i,j) matrix for various images indicate that coefficients (1,1) requires 9 bits allocated, which is the largest bit allocation. Approximately half the coefficients in the B(i,j) matrix require less than 3 bits. Those coefficients which contain less than 0.001/100 relative energy density are not transmitted. The statistical results also indicate that those coefficients which have the same bits allocation form hyperbolas in the B(i,j) matrix.

Statistical results also indicate that for most images coefficients (1,1) has an almost liner probability distribution, as shown if fig.8. Coefficients (16,8) and (16,9), in general, have a Laplace probability density. However, if an image contains only a constant hue or if it contains a specific hue which is strong, then the density will have its greatest value at some level other than that of the Laplace density.

The density of the other coefficients can be represented by a Laplace density with zero average value. The actual density may not be symmetric. The average value of the coefficient indicates the amount of skew. The majority of the coefficients have an average value close to zero. The density plots of coefficient (1,2) in the Walsh domain for the SMPTE #1 and SMPTE #4 test slides are shown in fig.9.

Thus, linear quantization is suitable for coefficients (1,1), (16,8), and (16,9) and any other coefficient which require 7 or more bits. Nonuniform quantization with a Laplace characteristic is suitable for all other coefficients which are to be transmitted.

SIMULATION OF CODEC

To simulate the codec a video image is first partitioned into data matrix and then each data matrix is transformed into a coefficient matrix using the Walsh transform. In order to obtain a good quality image at the receiver and maintain as low a bit rate as possible, it is necessary to find which coefficients of each matrix ought to be transmitted and how many bits are sufficient to code these coefficients. Three types of filter are used as shown in fig.10.

On the average, FIL10 requires 1.09 bits/sample, FIL15 requires 1.53 bits/sample and FIL18 requires 1.81 bits/sample. Table 2 shows the amount of energy that is transmitted by each filter. Note that the values in Table 2 do not take into consideration the quantization error. The number in these filters represent the number of bits required to code the corresponding coefficients. Coefficients requiring 7, 8 or 9 bits are coded using a uniform quantizer with quantization spacing of 0.5 if the largerst level allowed in the coefficient matrix is 256. Coefficients requiring less than 7 bits are coded using a nonuniform quantizer.

The coefficients which represent the lower frequency components of an image are assigned a larger number of bits because 1) they have larger energy and variance 2) the quantization noise in these coefficients are easily seen by human eyes, and 3) there are large changes in the average value of these coefficients from image to image so that a nonuniform quantizer is not suitable.

The result of using these three filters are shown in fig.11. The only degradation that is visiable when using FIL18 is that there is a small amount of noise.

The processed image with FIL10 has stairwave contouring at slanted edges and noticable resolution degradation. This is due to the fact that most of the coefficients which represent the details in an image are suppressed.

The processed image with FIL15 has substantial noise and little resolution degradation. The reason for this is that the coefficients are allocated a small number of bits and consequently the quantizer generates substantial amount of quantization noise.

In order to show that the coefficients (16,8) and (16,9) nearly represent the Q and I signals respectively, two other filters i.e. FILYQ and FILYI were used. These filters are the same as filter FIL18 except that coefficients (16,9), (16,10) and (15,9) are suppressed in FILYQ and coefficients (16,8), (16,7) and (15,8) are suppressed in FILYI. The image processed with FILYI is shown in fig.12. In this case the color vectors are all on the I axis of the vectorscope as shown in fig.13. All the color components in the processed image belong to two opposite hues.

CONCLUSION

We have shown that a NTSC composite signal can be decomposed into its YIQ components by applying a two-dimensional Walsh transform to a properly sampled NTSC composite color signal. In addition, the YIQ components are always mapped into fix locations of the coefficient matrix in the Walsh domain.

The advantage of this technique is that there is no loss of information that is normally associated with the use of comb filters in order to perform component coding of NTSC composite signals. The above results were extended to the PAL color system.

Examples of component coding were presented which yield very good picture quality at 1.8 bits/pixel. At these rates two digital NTSC television signals can be transmitted over a single 36 MHz. satellite transponder using QPSK modulation.

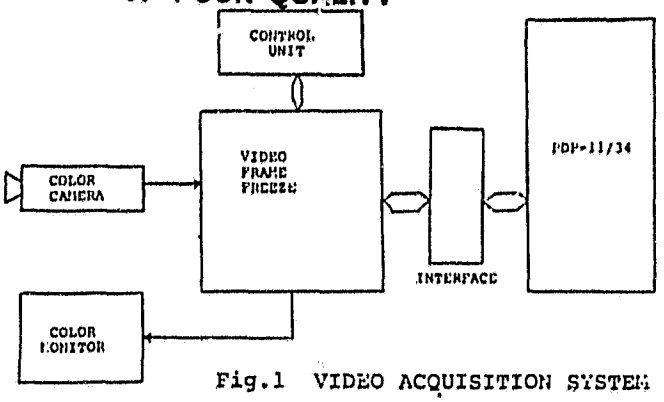

Fig.1 VIDEO ACQUISITION SYSTEM

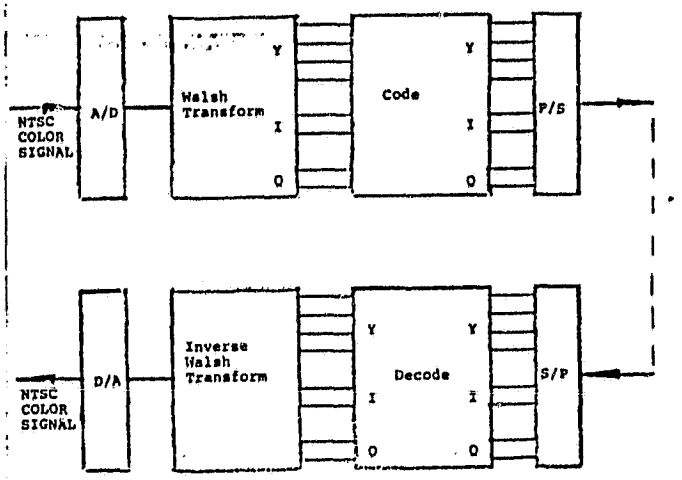

Fig.2 Block diagram of codec for NTSC signals

171.5	2.8	2.7	0.9	0.9	-0.7	1.4	0.2	0.5	-0.1	0.1	-0.2	0.4	-0.4	0.7	0.1
3.4	1.8	0.5	0.8	0.1	-0.1	0.1	0.6	0.2	-0.1	-0.1	0.0	0.0	0.0	0.1	0.2
-2.5	-2.6	1.1	-1.1	0.0	0.1	0.4	-0.4	0.2	0.1	-0.2	0.1	0.0	0.1	0.2	-0.2
-1.6	1.3	0.9	0.7	0.3	-0.2	0.4	0.5	0.3	-0.1	-0.1	-0.1	0.2	-0.1	0.1	0.1
-2.7	-0.8	0.6	-0.3	0.6	0.0	0.3	0.2	0.2	0.0	-0.1	0.1	0.0	0.1	0.1	0.0
-1.6	-0.3	0.0	-0.1	0.2	0.0	0.4	0.2	0.1	0.0	0.0	0.0	0.0	0.1	0.1	0.0
-2.1	-1.4	0.5	-0.6	0.1	0.2	0.3	0.0	0.3	0.0	-0.1	0.1	0.0	0.1	0.0	-0.1
-1.3	-0.1	0.3	0.0	0.1	0.1	0.3	0.3	0.2	0.2	0.0	0.1	0.0	0.0	0.1	0.1
-0.6	-0.7	0.0	-0.1	-0.2	-0.1	-0.2	0.0	-0.1	-0.2	-0.2	-0.2	0.0	0.0	-0.1	-0.1
-0.0	-0.1	0.0	-0.2	0.0	-0.1	-0.1	0.2	0.3	0.0	-0.2	0.0	0.0	0.0	-0.1	0.0
-0.5	-0.1	-0.1	-0.1	-0.1	-0.1	0.0	0.2	0.3	0.0	-0.2	0.0	0.0	0.0	-0.1	0.0
-0.4	-0.4	-0.1	-0.2	-0.1	-0.1	-0.2	0.1	0.3	-0.1	-0.2	-0.1	0.0	0.0	-0.1	-0.1
-1.1	-0.1	0.1	-0.1	-0.1	0.0	-0.2	-0.1	-0.1	-0.4	-0.1	-0.2	0.1	0.0	0.0	-0.2
-1.6	-0.1	0.3	-0.1	0.0	-0.3	0.0	0.2	0.2	0.2	-0.1	0.2	0.0	-0.1	-0.1	0.0
-0.9	-0.6	0.0	-0.4	0.0	-0.2	-0.2	-0.4	-0.7	-0.4	-0.1	-0.1	0.1	0.0	0.0	-0.2
-0.0	0.4	2.2	0.0	-0.1	0.2	-0.1	-2.6	4.1	-0.1	-0.1	-0.1	0.1	-0.1	0.0	-0.1

(a)

168.0	0.0	0.0	0.0	0.0	0.0	0.0	-0.1	0.1	0.0	0.1	0.0	0.0	0.0	0.0	0.0
-0.1	0.0	0.0	0.0	0.0	0.0	0.0	-0.1	0.0	0.0	0.0	0.0	0.0	0.0	0.0	0.0
0.0	0.0	0.0	0.0	0.0	0.0	0.0	0.1	0.1	0.0	0.0	0.0	0.0	0.0	0.0	0.0
0.0	0.0	0.0	0.0	0.0	0.0	0.0	0.1	-0.1	0.0	0.0	0.0	0.0	0.0	0.0	0.0
0.0	0.0	0.0	0.0	0.0	0.0	0.0	-0.1	0.1	0.0	0.0	0.0	0.0	0.0	0.0	0.0
0.0	0.0	0.0	0.0	0.0	0.0	0.0	0.0	-0.2	0.0	0.0	0.0	0.0	0.0	0.0	0.0
0.0	0.0	0.0	0.0	0.0	0.0	0.0	0.0	0.0	0.0	0.0	0.0	0.0	0.0	0.0	0.0
0.0	0.0	0.0	0.0	0.0	0.0	0.0	0.1	0.0	0.0	0.0	0.0	0.0	0.0	0.0	0.0
0.0	0.0	0.0	0.0	0.0	0.0	0.0	0.2	0.0	0.0	0.0	0.0	0.0	0.0	0.0	0.0
0.0	0.0	0.0	0.0	0.0	0.0	0.0	0.1	-0.1	0.0	0.0	0.0	0.0	0.0	0.0	0.0
0.0	0.0	0.0	0.0	0.0	0.0	0.0	0.0	0.0	0.0	0.0	0.0	0.0	0.0	0.0	0.0
0.0	0.0	0.0	0.0	0.0	0.0	0.0	0.0	0.0	0.0	0.0	0.0	0.0	0.0	0.0	0.0
0.0	0.0	0.0	0.0	0.0	0.0	0.0	0.0	0.1	0.0	0.0	0.0	0.0	0.0	0.0	0.0
0.0	0.0	0.0	0.0	0.0	0.0	0.0	0.0	-21.7	20.0	0.0	0.0	0.0	0.0	0.0	0.0

(b)

Fig.3 10th row, 10th col. coefficient matrix
(a) SMPTE #4 (b) COLOR BARS

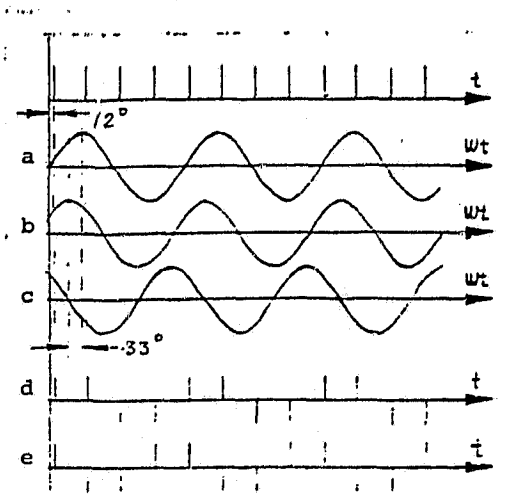

Fig.4 Phase relation of samples
(a) subcarrier (b) mod. Q
(c) mod. I (d) sampled Q
(e) sampled I

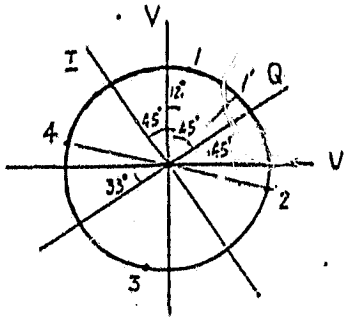

Fig.5 Locations of samples on color vector diagram

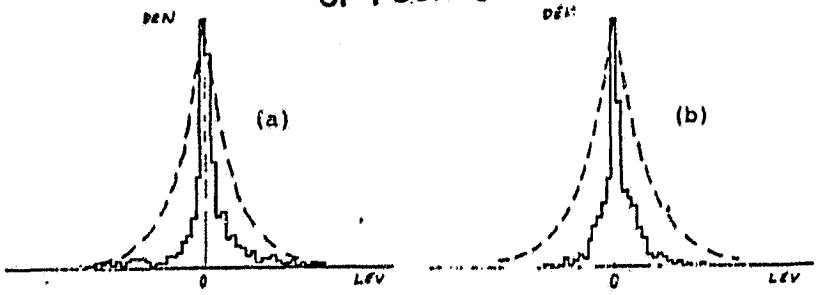

Fig.9 Level histogram of coefficient (1,2)
(a) SMPTE#4 (b) SMPTE#1

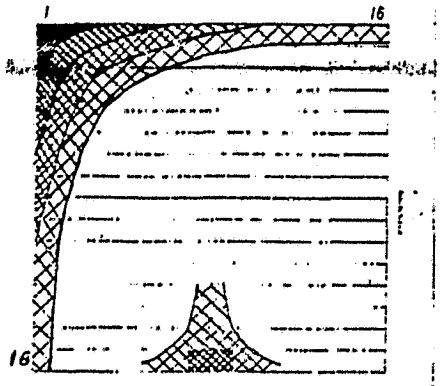

Fig.6 Energy distribution in coefficient matrix

	(16,8)	(16,9)	(1,1)
white	0.0	0.0	215
yellow	-21.7	20.0	168
cyan	-13.4	-40.8	148
green	-34.6	-20.2	136
magneta	35.2	19.3	117
red	13.9	40.0	104
burst	-17.3	10.2	60

TABLE 1 Color bars coefficients

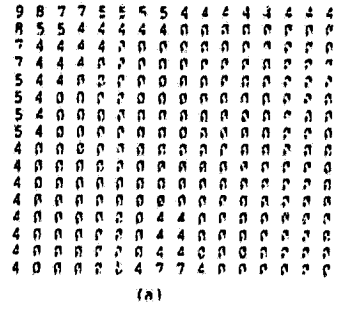

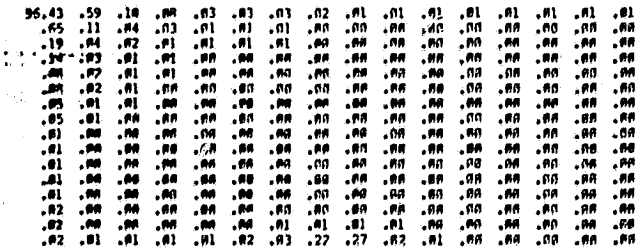

Fig.7 Energy distribution of SMPTE#1

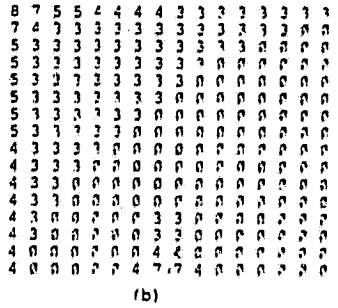

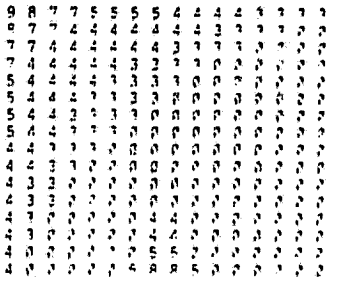

Fig.10 Three filters
(a) FIL10
(b) FIL15
(c) FIL18

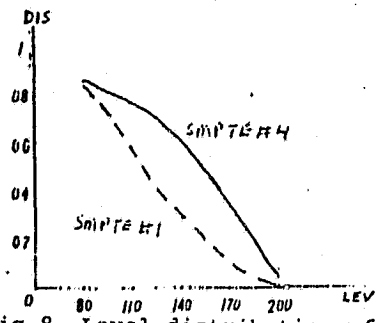

Fig.8 Level distribution of coefficient (1,1)

	SMPTE#1	SMPTE#4
FIL10	99.89	99.90
FIL15	99.94	99.96
FIL18	99.94	99.96

TABLE 2 Energy transmitted

(a)

(b)

(c)

(d)

Fig.11 Processed images: (a) original (b) FIL10 (c) FIL15 (d) FIL18

(a)

(b)

Fig.12 (a) original (b) FILYI

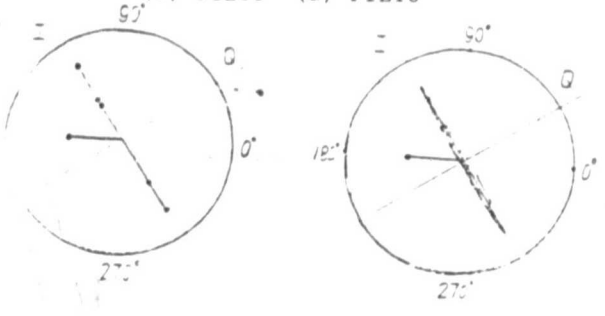

Fig.13 Processed with FILYI (a) burst (b) SMPTE-1

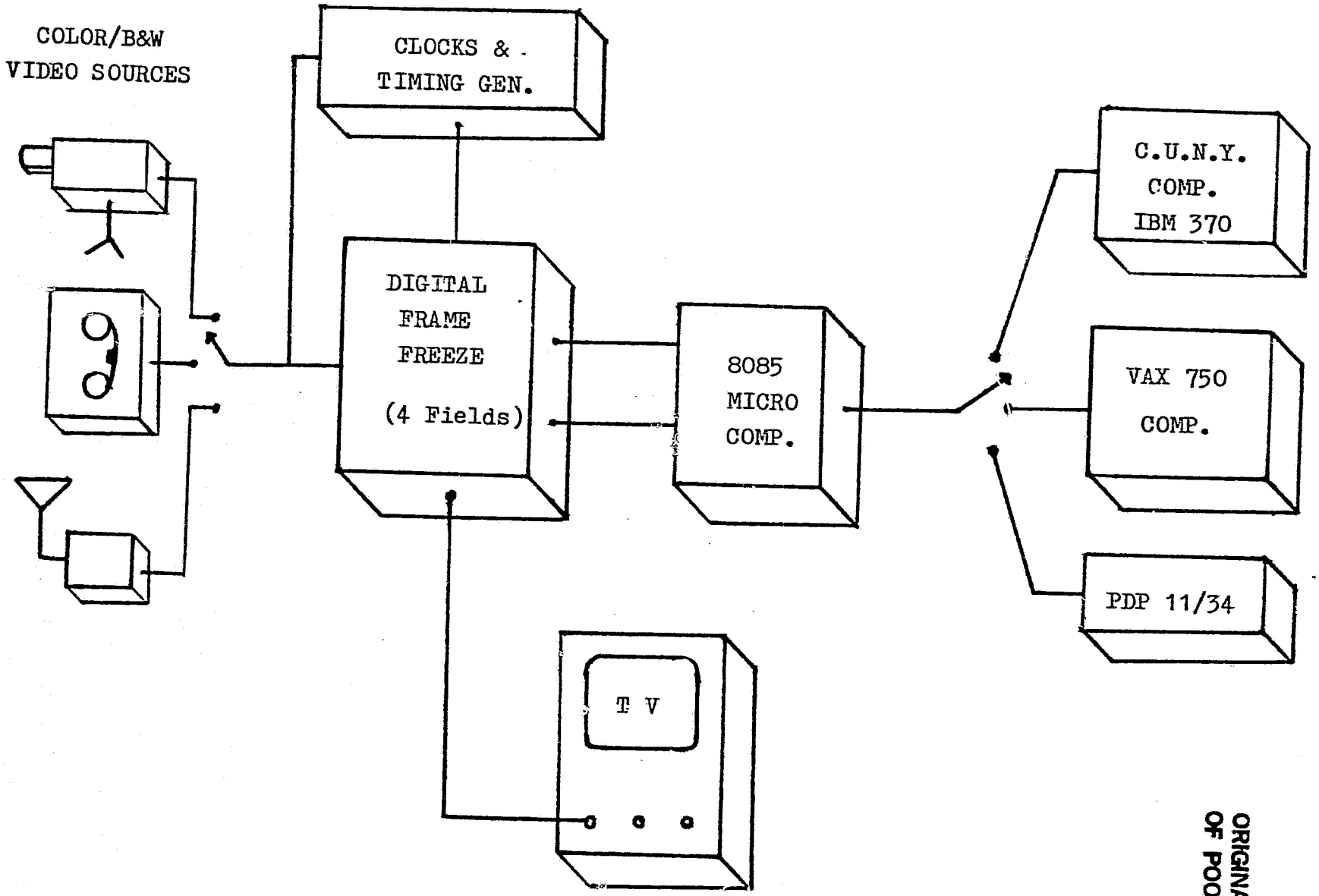

CITY COLLEGE IMAGE PROCESSING FACILITIES

ORIGINAL PAGE IS
OF POOR QUALITY